

Scanning tunneling microscopy of Bi_2Te_3 films prepared by pulsed laser deposition: from nanocrystalline structures to van der Waals epitaxy

N.I. Fedotov^a, A.A. Maizlakh^a, V.V. Pavlovskiy^a, G.V. Rybalchenko^b and S.V. Zaitsev-Zotov^{a,c}

^aKotelnikov Institute of Radioengineering and Electronics of Russian Academy of Sciences, Mokhovaya 11, bld. 7, Moscow, 125009, Russian Federation

^bP. N. Lebedev Physical Institute, Leninsky pr., 53, Moscow, 119991, Russian Federation

^cNational Research University Higher School of Economics, 20 Myasnitskaya Street, Moscow, 101000, Russian Federation

ARTICLE INFO

Keywords:

Bi_2Te_3
pulsed laser deposition
scanning tunneling microscopy
scanning tunneling spectroscopy
thin films
van der Waals epitaxy

ABSTRACT

Bi_2Te_3 is a material with high efficiency of thermoelectric energy conversion. Recently, it was also recognized as a topological insulator, and is often used as the basis for creation of other types of topological matter. Pulsed laser deposition (PLD) is widely considered as a simple method for growing of multicomponent films, but not as a tool for van der Waals epitaxy. We demonstrate here that the van der Waals epitaxy of Bi_2Te_3 is indeed impossible in vacuum PLD, but is possible in the presence of a background gas, which is confirmed by the results of scanning tunneling microscopy and spectroscopy studies. Results of *ab initio* calculations reproduce tunneling spectra of the first three terraces of epitaxial films of Bi_2Te_3 . In addition, an unusual hexagonal superstructure resembling a charge-density wave is observed in overheated films.

1. Introduction

Bi_2Te_3 is a layered material consisting of covalently bonded Te-Bi-Te-Bi-Te quintuple layers (QL) stacked along the c-axis to form a rhombohedral crystal. The quintuple layers are interconnected by a relatively weak van der Waals (vdW) interaction. This compound is widely known as a material with high efficiency of thermoelectric energy conversion [1]. In the last decade it has been also intensively studied as a topological insulator [2] – a novel type of solid state material and part of a larger class of topological materials, which includes magnetic topological insulators, various types of Weyl and Dirac semimetals, and topological superconductors. In general, their physical properties are determined by the presence of certain symmetries describing their band structures [3]. Topological insulators are characterized by the presence of a bulk energy gap and topologically protected edge or surface states. Presently, topological insulators Bi_2Te_3 and Bi_2Se_3 remain the most popular topological materials and even are often used as the basis for creation of other types of topological matter. For instance, by proper doping they can be transformed into topological superconductors [4] or a magnetic topological insulator [5].

The structure of films for thermoelectric applications and of those suitable for the use of their topological properties must satisfy different requirements. The films of interest for thermoelectric applications should contain a large number of grain boundaries that prevent phonon propagation. Meanwhile, for topological applications, high quality continuous films or isolated islands are the most appealing.

In thin films of topological materials, a number of exotic states can be realized, such as a quantum spin Hall state, an axion insulator, an anomalous quantum Hall state, as well as numerous effects at the boundaries of films, islands, and grains [6]. One way to obtain thin films of layered topological materials would be mechanical cleaving along weak vdW bonds using micromechanical cleavage [7]. This technique is usually used for obtaining clean surface of bulk crystals, and also was heavily utilized in early graphene studies. However, it is poorly scalable for industrial usage. Therefore more and more attention has been paid to methods for growing thin films of vdW materials, such as vdW epitaxy [8, 9]. Due to very low surface energy of vdW materials, it allows thin films to be grown without meeting the requirements for lattice matching between substrate and film, especially if substrate is also a vdW material.

One way to achieve vdW epitaxy is to employ widely used molecular beam epitaxy (MBE) and use a substrate without dangling bonds. To date, there exist a number of reports detailing various ways to grow Bi_2Te_3 (see for instance [10–16]). In all mentioned works the substrate was heated to a temperature $T_s=170\text{--}350$ °C during the deposition process. The heating provides surface adatom mobility and allows the formation of large single-crystal films. However, it also results in tellurium deficiency due to high vapor pressure of Te at those temperatures. An excess tellurium flux is required to maintain stoichiometry of Bi_2Te_3 . The typical beam equivalent pressure (BEP) ratio of Te_2 flux to Bi flux was around 20 in most cases. It was also shown that a higher T_s requires higher BEP ratio.

One notable example of MBE growth of Bi_2Te_3 film is described in Ref. [16]. In this work, one effusion cell was loaded with Bi_2Te_3 instead of pure Bi. The resulting BEP for Te_2 flux to Bi_2Te_3 flux is given as 2, which corresponds to Te_2 flux to Bi flux ratio of 1.75. The growth was performed

✉ SerZZ@eplire.ru (S.V. Zaitsev-Zotov)

ORCID(s): 0000-0001-6145-109X (N.I. Fedotov); 0000-0002-5942-1323 (S.V. Zaitsev-Zotov)

on highly oriented pyrolytic graphite (HOPG). Such a combination of low BEP ratio with the high surface adatoms mobility substrate provides the lowest optimal $T_s = 170$ °C. In addition, obtained films were as thin as 1.4 QL (given that 1 QL is roughly 1 nm, the thickness therefore is 1.4 nm). The results could be considered a fine example of vdW epitaxy by MBE.

Aside from MBE, another promising method to achieve vdW epitaxy is pulsed laser deposition (PLD) [17]. It is a relatively easy way to produce multi-component films. However, early works [18, 19] regarding PLD of Bi₂Te₃ show that deposition of films in vacuum $< 10^{-7}$ Torr results in Te deficiency. The issue persists even when a substrate is at room temperature. The effect is largely attributed to Te plume expansion and plume-laser beam interaction. A consistent way to prevent Te loss is to introduce inert gas into the chamber during deposition, as shown by Bailini, *et al.* [19]. This and later works use Ar at a pressure of 1.5×10^{-2} - 3 Torr [19–26] or He at 2×10^{-5} – 2×10^{-3} Torr [27] for this purpose. Optimal substrate temperature varies between 200 to 300 °C. In [19] it is also shown that correct stoichiometry of the film can be obtained due to thermal evaporation of extra Te if a target with Te excess is used.

This work presents the results of STM studies of films grown in a two-step process both in vacuum and argon atmosphere at different substrate temperatures and further annealing in vacuum. As a substrate in our experiments, we used highly oriented pyrolytic graphite (HOPG), which has the conductivity required for using STM, the same rotational symmetry, no dangling bonds and therefore being vdW material appropriate for vdW epitaxy. The results obtained indicate the possibility of controlling the film morphology by choosing deposition and subsequent annealing conditions and provide recipes for fabrication of films with the surface morphology required. We demonstrate also that PLD in vacuum results in substrate damage and therefore cannot be used for vdW epitaxy. Instead, PLD at a moderate inert gas pressure followed by annealing at temperatures 150–200 °C provides vdW epitaxy of ultrathin crystalline films of Bi₂Te₃.

2. Methods

A home-made PLD setup connected to the Omicron LT SPM by a vacuum transport channel through an additional technological chamber (XP chamber) was used for film deposition. Laser radiation was focused into a spot 1 mm in diameter on a target with a typical size of 10×15 mm. The target was scanned using a computer-controlled lens positioning system providing typical scanning rate of 100 mm/min, which ensured that there was no overlap between the light spots. The second harmonic ($\lambda = 532$ nm) of a neodymium laser working at a repetition rate of 0.2 - 0.5 Hz with 7 ns pulse duration and 80 - 82 mJ pulse energy was used. The target-substrate distance was 5 cm. The nominal deposition rate was 2.5 Å/min. The amount of deposited material was controlled by a quartz microbalance

located next to the substrate holder. The base vacuum in the deposition chamber was $1 - 2 \times 10^{-8}$ Torr and it deteriorated to $\sim 10^{-7}$ Torr in the process of deposition. Prior to every deposition, HOPG substrate was cleaved *ex situ* and annealed in vacuum at $T = 430$ °C during at least 1 hour. The temperature of the substrate in the PLD chamber was measured with a thermocouple calibrated with a thermistor glued by conductive carbon paint at substrate position, the calibration curves for vacuum and argon being different. Post-deposition annealing was carried out in ultra-high vacuum conditions in the Omicron XP chamber. The temperature regime during deposition and subsequent annealing was maintained automatically. STM/STS study was performed in LT STM chamber at pressure 2×10^{-11} Torr and temperature 78 K. Typical set points for STM images and STS spectra collection are ± 0.5 V and 0.2 nA.

The elemental composition of the films was investigated using SEM-EDS analysis performed on films with a nominal thickness of 100–150 nm in order to reduce the contribution of the substrate. JSM-7001F scanning electron microscope (JEOL) with an energy-dispersive X-ray analyzer (INCA-act Oxford Instruments) and INCA software was used. The EDX spectra were obtained using 20 kV accelerating voltage and beam current of about 0.07 mA. The average sample composition was calculated after at least ten point measurements during 1800 sec each. It is important to note that the distribution of Bi and Te in each thin film was additionally analyzed by element mapping during several hours.

The electronic band structure was calculated using density functional theory (DFT) with the local-density approximation (LDA) and spin-orbit interaction taken into account. A preliminary structure optimization was performed for each structure using $8 \times 8 \times 1$ \vec{K} -mesh.

For the STM spectra calculations Tersoff-Hamann approximation [28] was used, according to which STM differential tunneling conductance is proportional to the local density of states (LDOS) $N(\vec{R}, E)$

$$N(\vec{R}, E) = \sum_{\nu} \left| \psi_{\nu}(\vec{R}) \right| \delta(E - E_{\nu}), \quad (1)$$

where $\psi_{\nu}(\vec{R})$ is the wave function at the point of the tip location \vec{R} and E_{ν} is the corresponding eigenenergy.

Tip location was chosen at a proper distance from the surface of the slab in the vacuum gap, where wave functions demonstrate an exponential decay. Pseudo wave functions in this area coincide with true electron wave functions and the influence of slab's opposite surface is rather low. Dirac's δ -function was approximated by Lorentz's function with 40 meV width, which corresponds to the voltage resolution of STM. Pseudo wave functions were calculated using optimized slab crystal structures on $24 \times 24 \times 1$ \vec{K} -mesh.

3. Preliminary notes

The choice of the target composition may affect the deposition results. When using the MBE method, sources

providing 8-20 time larger Te over Bi fluxes are required at substrate temperature 200-600 °C [10, 29]. In the PLD method realized in vacuum conditions some tellurium loss also occurs, so targets with extra tellurium content over stoichiometry are also required [19]. From the Bi-Te phase diagram [30] we expect the films at more than 60 at. percent Te to consist of two phases: Te and Bi₂Te₃. Given the high vapor pressure of Te we expect it to evaporate upon annealing, leaving only Bi₂Te₃ behind.

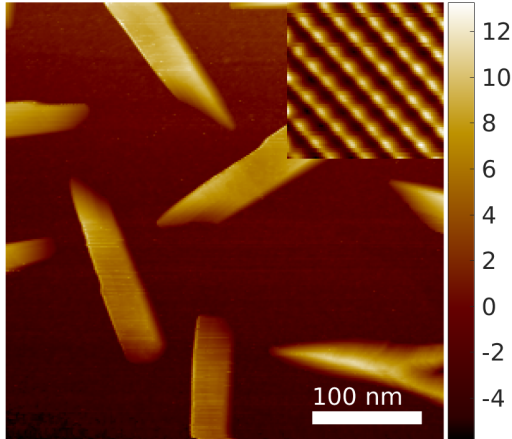


Figure 1: STM image of a Te film deposited at substrate temperature 120 °C in vacuum. Inset shows a fragment of atomically resolved surface of the central crystallite.

We have undertaken a test deposition of tellurium to study the effect of annealing. The results are shown in Fig. 1. Tellurium deposited at a substrate temperature of 120 °C aggregates in large crystals with the atomic structure corresponding to β -Te [31] (see the inset) whereas it forms a continuous amorphous film if it is deposited at 60 °C. Amorphous film becomes polycrystalline upon annealing at 120-175 °C and evaporates from the HOPG substrate as a result of annealing at $T \gtrsim 240^\circ\text{C}$. Thus the amount of tellurium can be adjusted to proper stoichiometry of the film by choosing the substrate temperatures during deposition and subsequent annealing below 300 °C. In the present work, we used a target with an atomic ratio of components Bi/Te = 1/5 which allows us to deposit films with both over and under stoichiometry amount of tellurium.

The phase of our interest Bi₂Te₃ is the most stable one as it has the minimum formation energy among other phases. The other ones, described by the formula (Bi₂)_n(Bi₂Te₃)_m, consist of alternation of Bi₂Te₃ quintuple layers with bismuth bilayers. Some examples are BiTe [32] (which is also a topological insulator [33]), Bi₄Te₃ [32] *etc.* They are formed when the content of tellurium in the system is less than 60 percent.

Phase identification of ultra-thin Bi-Te films by STM can be done by study of atomic structure of film surface, heights of terrace steps and scanning tunneling spectroscopy (STS) spectra. The main phases that may appear are bilayers of Bi, quintuple layers of Bi₂Te₃, septuple layers (SL) of Bi₄Te₃, with thicknesses 0.34, 1.01 and 1.35 nm respectively. All

these phases have hexagonal symmetry of surface atomic structure with very close interatomic distance values which are hardly distinguishable by STM, but their energy structures are different.

4. Results

4.1. *ab initio* calculations

STM spectra were calculated from the results of *ab-initio* band structure calculations. In order to build crystal structures which are suitable for the surface electronic structure investigation we used unit cells of Bi₂Te₃ and Bi₄Te₃ compounds with hexagonal axes as basic structures. Structure parameters were taken from [34]. Slab structures with the boundaries required were cut from the base structures along the z plane with vacuum gaps added.

The following slab structures were used:

- (i) one, two and three Bi₂Te₃ QLs with Te layer surface and the vacuum gap above;
- (ii) three Bi₂Te₃ QLs cleaved between 2-nd and 3-rd layer of the central QL and the vacuum gap in the break;
- (iii) one SL of Bi₄Te₃ with Bi bi-layer at the surface and the vacuum gap above;

Structures (ii) and (iii) correspond to different types of Bi₂Te₃ surfaces with abnormal terminations which can also be observed experimentally [35]. The geometry of the three QL unit cell with a break in the middle was chosen for the structure (ii) to exclude electrical polarization of the unit cell. It is shown as a continuous slab with abnormal terminated surfaces in fig. 2b below. Vacuum gap width of 16 Å and 3 Å distance of the tip and the surface were used for all structures. Main expected structures used for calculations are presented at Fig. 2(a-c). These pictures were prepared with the usage of Vesta program [36].

Fig. 2(d-j) shows local density of states (LDOS) calculated for the main expected structures.

As all the spectra are very different, so their control may help to distinguish grown structures.

4.2. Vacuum Deposition

4.2.1. Annealing of films deposited at 60 °C

EDS analysis of films deposited at 60 °C gives Te/(Bi + Te) = 0.65 for relative tellurium content, that is slightly above the required 0.6 atomic percent ratio for Bi₂Te₃. Fig. 3(a) shows an STM image of a film deposited at 60 °C. The film consists of small terraced crystallites with typical sizes 10-20 nm. The characteristic terraces height on top of the grains is 0.3-0.4 nm, which is significantly less than the thickness of the Bi₂Te₃ quintuple layer.

Heating this film to 100 °C for an hour does not lead to significant changes in its topography. However, one hour annealing at 150 °C results in a noticeable growth of lateral grain sizes (Fig. 3 (b)), and grains merge into a continuous film upon further annealing at 250 °C (Fig. 3 (c)). All the structures obtained with this film in the annealing process at temperatures not exceeding 250 °C look flatter and more interconnected than for films deposited at higher substrate

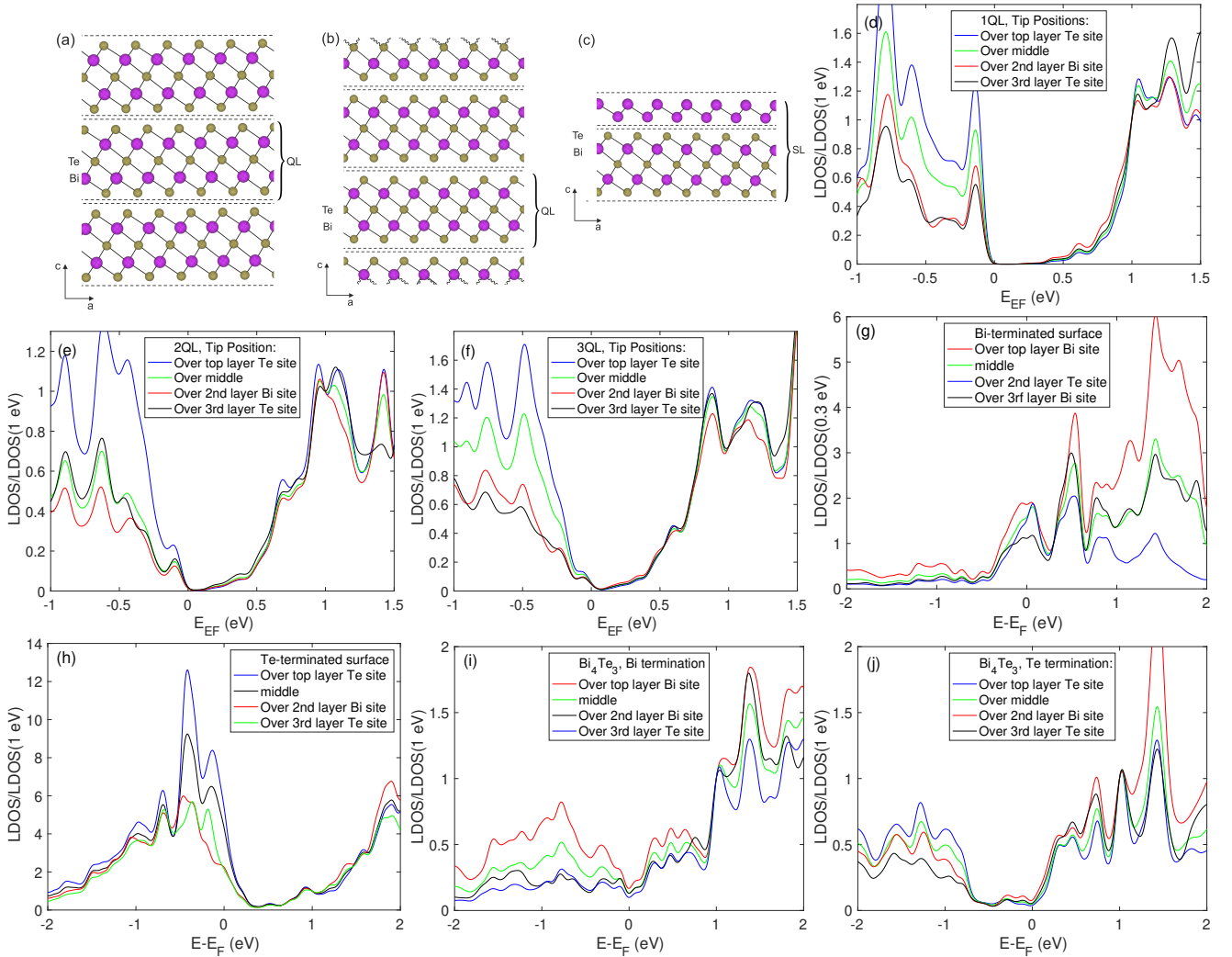


Figure 2: (a-c) Slab structures used for calculations: (a) 3QL slab; (b) a slab with abnormal Bi-terminated and Te-terminated surfaces; (c) 1SL of Bi_4Te_3 slab. Chemical bonds are indicated by solid lines for covalent, double dashed lines for vdW, single dashed lines for broken vdW and wavy lines for broken covalent bonds. The tip Z-position is 3 Å over the upper surface. LDOS of: (d) 1QL Bi_2Te_3 ; (e) 2QL Bi_2Te_3 ; (f) 3QL Bi_2Te_3 . (g,h) LDOS of Bi_2Te_3 slab with abnormal terminated surfaces: (g) Bi-terminated surface; (h) Te-terminated surface. LDOS of 1SL of Bi_4Te_3 for (i) Bi- and (j) Te-terminated surfaces.

temperature (see below). Surprisingly, the STS spectra of as-deposited and annealed films remain unchanged (Fig. 3(d)) and resemble the STS spectrum of bulk Bi_2Te_3 (Fig. 2(f)).

An increase in the annealing temperature to 300 °C leads to the disintegration of the continuous film into separate islands 6-10 nm in height (see also results for higher deposition temperatures).

4.2.2. Annealing of films deposited at 175 °C and 240 °C

Films deposited at 175 °C and 240 °C consist of individual grains with different orientations (Fig. 4(a)). Their faceting corresponds to the presence of symmetry axes of the 3rd order. Terraces with heights of 0.3-0.4 nm are usually observed on the upper surface of the grains. The films deposited at 240 °C have a more ordered structure and larger crystallites than films deposited at 175 °C after annealing for the same duration at the same temperatures. In addition,

the crystallites are more disordered in films deposited at a substrate temperature of 175 °C, than in films deposited in a vacuum at 240 °C.

Annealing of the films at temperatures no higher than 250 °C leads to a gradual increase in grain sizes Fig. 4(a,b) with hexagonal symmetry of the top surface (inset in Fig. 4(b)). Heating the film to 300 °C for one hour changes the picture - the grains become solitary - and also opens the surface of the substrate, which is a disordered layer (Fig. 4(c)). Annealing at $T = 350$ °C results in disappearance of the grains but not of the disordered layer (Fig. 4(d)).

The grains are 6-8 nm in height and the atomic structure on their tops remains almost unchanged and has hexagonal symmetry, in accordance with observed grain faceting. In general, the observed behavior corresponds to growth of Te-deficient structures such as $(\text{Bi}_2)_n/(\text{Bi}_2\text{Te}_3)_m$ ($n > 0$).

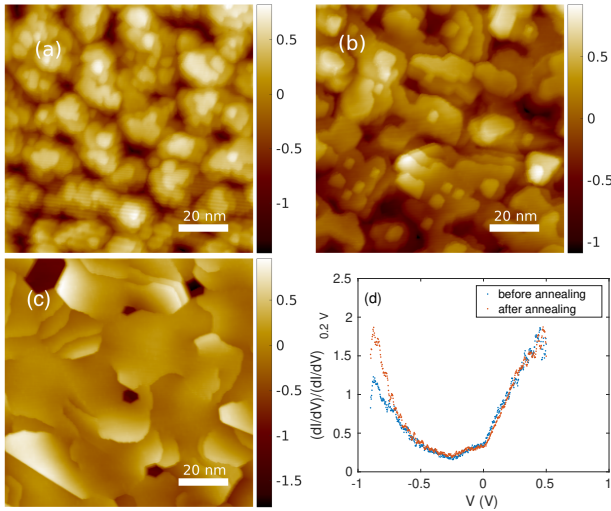


Figure 3: STM images of a film deposited at substrate temperature 60 °C (a) and annealed 1 h at (b) $T_a = 150$ °C, (c) 250 °C (color scales are in nanometers). (d) Comparison of STS spectra of as-deposited and annealed at 250 °C films.

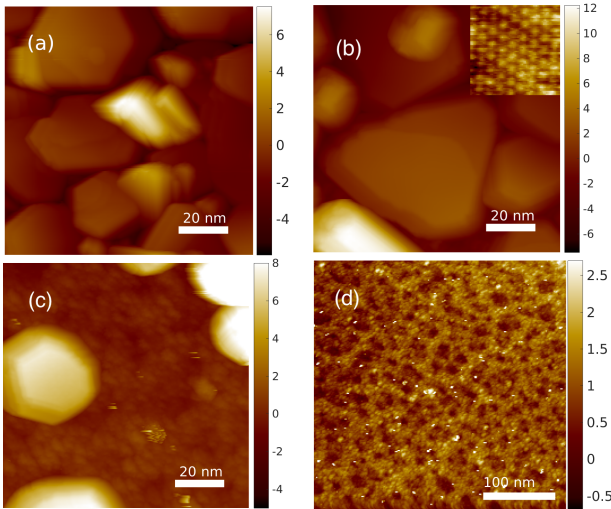


Figure 4: (a) STM image of a film deposited in vacuum at substrate temperature $T_d = 240$ °C. STM images of the film after 1 hour annealing at $T_a = 250$ °C (b) (inset shows typical image of crystallite surface with atomic resolution at tip current 0.2 nA and sample bias -0.5 V), $T_a = 300$ °C (c), and $T_a = 350$ °C (d). Color scales are in nanometers.

To summarize, PLD under vacuum conditions allows us to grow polycrystalline films of Bi_2Te_3 with grain sizes varying from tens to few hundreds of nanometers. Subsequent annealing in the temperature region 150-350 °C leads to growth of lateral grain sizes, then formation of sets of independent grains and finally to complete sublimation of crystallites leaving a disordered layer. The presence of this layer and varying orientations of the crystallites indicate chemical interaction of the film with the substrate surface and thus the absence of vdW epitaxy. We attribute this fact to the damage by the high-energy ions produced in the process of the laser ablation of the target. Their energies may reach

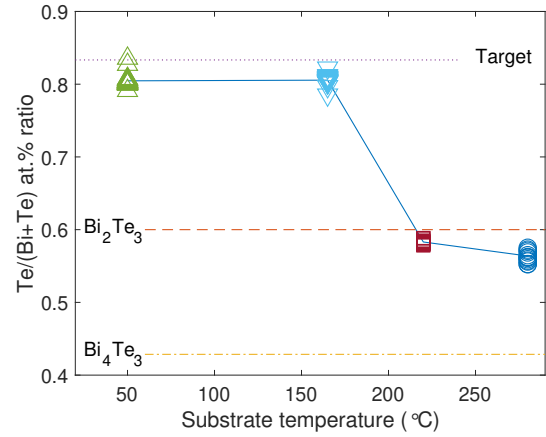


Figure 5: Atomic composition of films deposited by PLD under 0.3 Torr of argon at different temperatures.

hundreds eV, as was reported in [37]. Such high-energy ions would damage the substrate, thereby impairing the vdW epitaxy capability.

4.3. Deposition in argon

A way to avoid direct ion bombardment of a substrate is to perform PLD in the presence of an inert background gas. The effect of argon background gas pressure on the results of PLD of Bi_2Te_3 was reported earlier [19]. The best quality of films was achieved at an argon pressure of 40 Pa (0.3 Torr). So we also used argon at a pressure of 0.3 Torr as a background gas for the present study. As the room-temperature mean-free path is below 1 mm at this pressure, such a pressure is enough to exclude completely the high-energy ion damage of the substrate.

Fig. 5 shows the atomic composition of thick films (typical nominal thickness 100 nm) deposited in argon at different substrate temperatures. The films deposited at $T \lesssim 165$ °C show very little Te loss with respect to the composition of the target, that is they contain a large excess amount of Te. At the same time, the films deposited at $T \gtrsim 220$ °C exhibit a slight Te deficiency. These data are in agreement with our preliminary Te deposition experiments.

4.3.1. Annealing of films deposited at 50 °C

Films deposited at 50 °C consist of crystallites 5-10 nm in lateral sizes (Fig. 6(a)). The EDS analysis gives the presence of excess tellurium with $\text{Te/Bi} = 4.1 \pm 0.05$ atomic percent ratio (Fig. 5). Subsequent annealing for 1 hour at 100 °C leads to a slight increase in the size of crystallites. Further annealing for 1 hour at 150 °C does not fundamentally change the picture. Crystallites with the atomic structures characteristic of Bi_2Te_3 as well as Te can be observed.

The morphology of the film remains almost the same for $T_a \lesssim 200$ K and starts to change significantly after annealing at $T_a = 250$ °C and above. After annealing at $T_a = 250$ °C, the crystallites acquire a finished faceting, and for $T_a = 300$ °C, the film becomes flat and continuous. It also partially evaporates, uncovering intact HOPG surface.

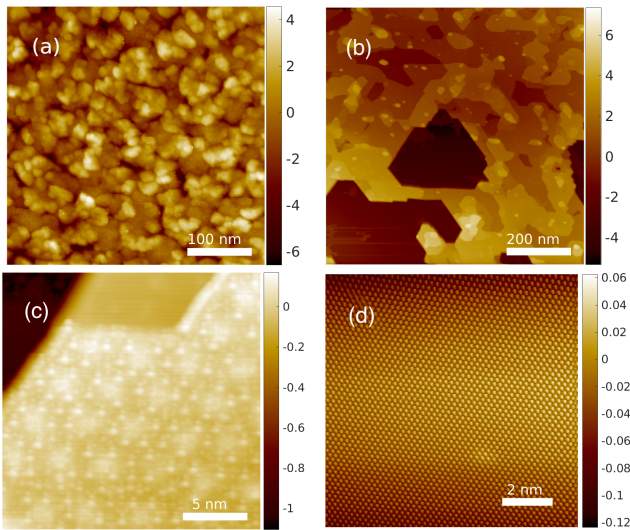


Figure 6: (a) STM image of a film deposited at substrate temperature 50 °C at argon pressure 0.3 Torr; the same film after annealing at $T = 300$ °C (b,c), and $T = 350$ °C (d) (color scales are in nanometers).

The terrace edges become straight, and faceted holes in the films develop (Fig. 6(b)). In this case, the orientation of the boundaries of the terraces corresponds to the orientation of the graphite substrate. Thus, the graphite substrate has an orienting effect on the film, despite the mismatch between the lattices of the substrate and the film. The surface of the films annealed at 300 °C shows indications of partial film decomposition, namely spots of rough surfaces with very interesting atomic ordering (Fig. 6(c)). The origin of such an ordering remains unclear and may be a manifestation of charge-density waves (CDW) with the wave vector 1.6 nm^{-1} accompanied by a surface reconstruction. Further heating up to 350 °C leads to complete evaporation of the films, leaving a clean substrate surface (Fig. 6(d)). Thus, the use of background gas during PLD not only promotes more adequate transfer of the target material to the substrate, but also protects the original structure of the substrate.

4.3.2. Annealing of films deposited at 165 °C

Films deposited at 165 °C in argon atmosphere demonstrate formation of large crystallites with well defined faces in addition to a continuous film (Fig. 7(a)). Their typical heights are few tens of nanometers and correlate with their cross-section area in agreement with the Gibbs-Wulff theorem. The crystallites have the same orientation of faces. We attribute their formation to the excess tellurium.

The continuous film consists of small terraces that form a discrete hilly relief. The faces of terraces are not well defined and have a wavy shape.

One hour annealing of the film at 200 °C leads to almost complete disappearance of the large crystallites and formation of a film with ≈ 1 nm height terraces. Further annealing at 250 °C during 1 hour leads to further growth of holes down to the substrate surface without noticeable change of the film

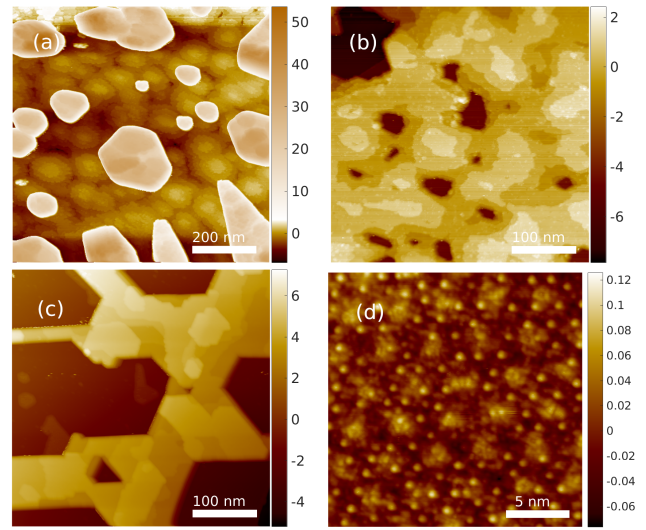


Figure 7: (a) STM image of a film deposited at substrate temperature 165 °C at argon pressure 0.3 Torr; The same film after 1 hour annealing at (b) 250 °C, and (c) 300 °C; (d) the upper surface of the film after annealing at 300 °C. Color scales are in nanometers.

thickness (Fig. 7(b)). The dominating terrace height remains to be ≈ 1 nm.

The final 1 hour annealing at 300 °C leads to formation of a crystalline mesh (Fig. 7(c)). The height of the mesh ≈ 5 -6 nm is still very close to the initial value of the film thickness (Fig. 7(a,b)), but the structure of the upper surface (Fig. 7(f)) demonstrates the same atomic reconstruction as films deposited at 50 °C and annealed at 300 °C (Fig. 6(c)).

Film diagnostics is convenient to perform on thinner films consisting of a few QL. Fig. 8(a,b) shows STM images of such a film. It consists of partially coalesced islands. The islands consist of three layers after annealing at 200 °C (Fig. 8(a)). The heights analysis (Fig. 8(c)) gives SL thickness for the first one and QL thickness for the next two. Annealing at 250 °C results in merging of the first two layers (Fig. 8(b,d)). STS data of the substrate, 1st, 2nd and 3rd layers are shown in Fig. 8(e-h) respectively. The data demonstrate very good correspondence to the calculated spectra for 1, 2, and 3QL (Fig. 2(d-f)) respectively.

4.3.3. Annealing of films deposited at 220 °C

Fig. 9(a) shows a typical STM image of a film deposited at $T_d = 220$ °C. The film consists of well-developed terraces with typical thickness 1 nm which corresponds to 1 QL of Bi_2Te_3 . Tunneling LDOS of the film (Fig. 9(d)) corresponds to LDOS of Bi_2Te_3 (Fig. 2(f)) with the chemical potential level inside the bulk band gap. The main difference between the films deposited at $T_d = 220$ °C and deposited at smaller temperature and annealed at $T > 200$ °C is that the latter have a tendency to grow as a set of islands, whereas the former form quasi-continuous layers.

One hour annealing of the film at $T_a = 250$ °C gives the same effect as is observed in films deposited in argon at 50 °C and annealed at 250 °C. Namely, the terrace boundaries

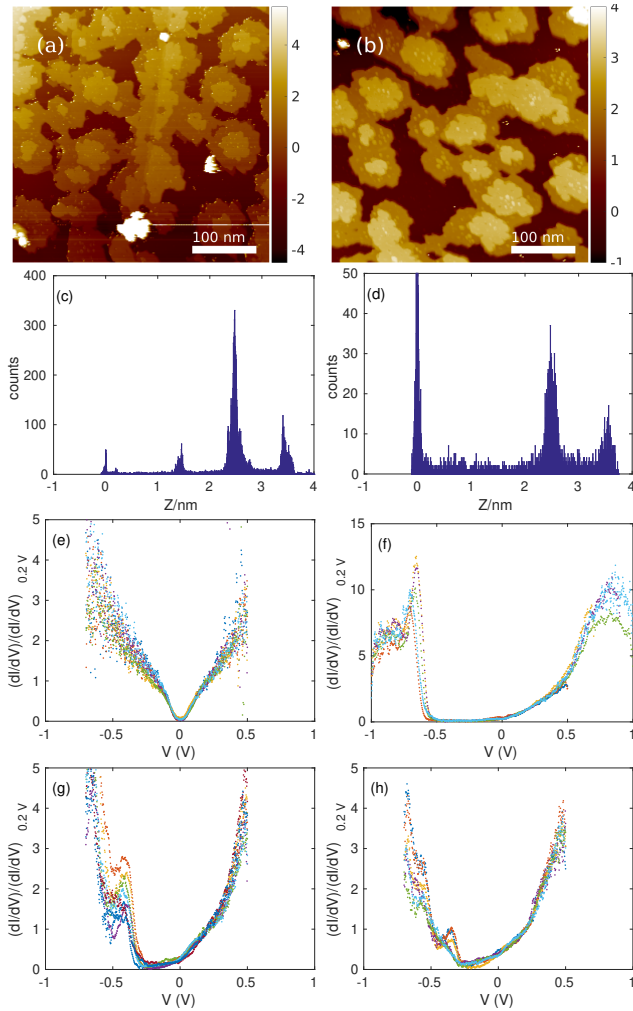


Figure 8: STM images of a thin film deposited at 165 °C and (a) annealed at 200 °C; (b) further annealed at 250 °C (color scales are in nanometers). (c),(d) - typical height distribution histograms of the film shown in (a), and (b) respectively. STS spectra of ultrathin films deposited at 165 °C and annealed at 200 °C collected at different levels: (e) substrate level; (f) first terrace; (g) second terrace; (h) third terrace.

are getting more and more flat and a hole structure down to the substrate starts to develop.

4.3.4. Deposition at 280 °C

Fig. 10(a) shows STM image of $800 \times 800 \text{ nm}^2$ region of a film deposited at argon pressure 0.3 Torr. The film consists of islands whose thickness is a multiple of QL thickness (Fig. 10(b)). Some islands coalescent forming a percolative crystalline network. The island height correlates with their width, in agreement with the Gibbs-Wulff theorem. In the presence of the macroscopic substrate defects (folds, steps), the film grows along such defects (Fig. 10(b)). Atomic structure of terrace surfaces has hexagonal symmetry, with triangular defects characteristic of Bi_2Te_3 (Fig. 10(c)). In addition, we observed small regions of surface degradation accompanied by superstructure development (Fig. 10(d))

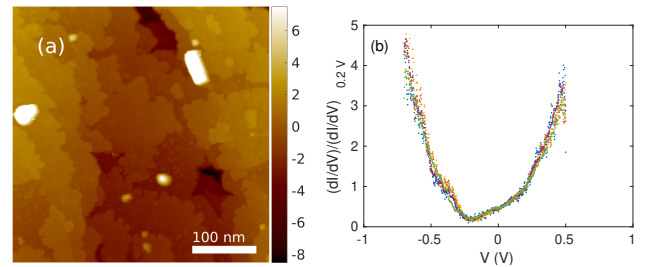


Figure 9: (a) STM image of a film deposited at substrate temperature 220 °C and argon pressure 0.3 Torr (color scale is in nanometers); (b) LDOS of the film.

similar to the ones observed in films deposited at lower temperatures and annealed at 300 °C (see Fig. 6(c), Fig. 7(d)). The LDOS on such surfaces (Fig. 10(f)) does not correspond to LDOS observed on undamaged surface and resembles the LDOS of Bi-terminated cleaved surface (Fig. 2(i)).

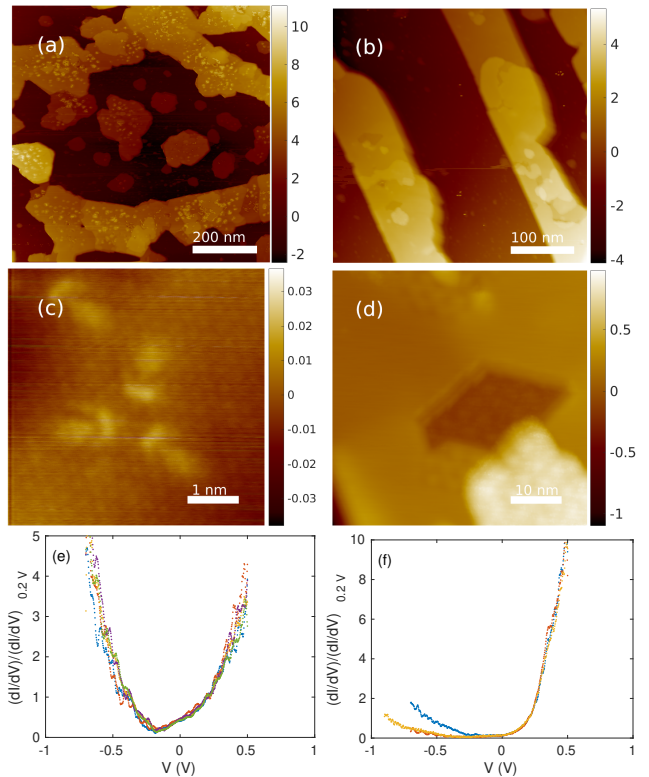


Figure 10: (a) $800 \times 800 \text{ nm}^2$ STM image of a film deposited at substrate temperature 280 °C at argon pressure 0.3 Torr and annealed in UHV conditions during 1 hour; (b) STM image of the film annealed at 300 °C; (c) STM image of a typical defect; (d) surface degradation region (color scales are in nanometers). (e) LDOS of a flat surface. (f) LDOS of reconstructed regions.

5. Discussion

As it can be seen from the results, thin polycrystalline Bi_2Te_3 films on the surface of pyrolytic graphite can be obtained by the PLD method in a surprisingly wide range

of substrate and subsequent annealing temperatures. Films deposited in vacuum from a target with an atomic ratio of components Bi/Te = 1/5 at a substrate temperature of 60–240 °C are polycrystalline with grain sizes of 10–50 nm and a random orientation of crystallites. Such polycrystalline films may be of interest for thermoelectric applications.

An interesting behavior is observed for films deposited in vacuum at a substrate temperature of 60 °C. The crystallites in these films are more ordered than for films deposited at higher temperatures. Annealing of these films at temperatures above 200 °C leads to the formation of a quasi-continuous wavy structure resembling potato chips. The appearance of such a structure can be explained by the accretion of crystallites with different inclination relative to the substrate surface and opens up a possibility to study the effect of very strong crystal distortion on its electronic properties. This effect is not observed in films deposited at 175 and 240 °C apparently because of lack of tellurium in as-deposited films.

A common feature of all the films is a noticeable sublimation of crystallites during annealing at temperatures of 300 °C and higher. After complete disappearance of the film, a disordered layer remains on the substrate, which is not expected for the case of vdW epitaxy. We attribute the appearance of this layer to the presence of high-energy ions during laser sputtering of the target, which damage the substrate.

To eliminate the destructive effect of high-energy ions on the substrate, we carried out experiments on the deposition of films in an argon atmosphere at a pressure of 0.3 Torr. The small value of the mean free path at this pressure (less than 1 mm) ensures the absence of high-energy ion collisions with the substrate. The films obtained as a result of such deposition and subsequent annealing at $T_a \gtrsim 200$ °C turn out to be highly crystalline, and after their sublimation, an intact atomic structure of HOPG is recovered. Thus, the vdW epitaxy with PLD is only possible when laser ablation occurs in inert gas atmosphere.

PLD in argon atmosphere at moderate substrate temperatures also results in a more congruent material transfer from the target. In our case, this corresponds to a high Te content, with the excess Te spreading uniformly or forming large crystallites depending on the substrate temperature during deposition. Annealing at $T_a \gtrsim 200$ °C results in evaporation of the excess Te.

The energy structure of the films corresponds to the structure of the topological insulator Bi₂Te₃. In particular, STS spectra of the first three terraces of the film correspond to calculated LDOS of 1QL, 2QL and 3QL respectively. The heights of the second and third layers correspond with the expected height of 1 QL, while surprisingly the height of the first layer is larger and indicates the presence of a buffer layer.

We have also observed that annealing at $T_a \approx 300$ °C results in development of a hexagonal atomic superstructure with a 4 nm period. The STS measurements indicate the presence of an energy gap at the Fermi energy, as it is

expected in the case of the CDW transition. The origin of this CDW-like reconstruction requires further study.

6. Conclusion

In conclusion, the morphology and chemical composition of nanometer-scale thickness Bi-Te system films grown by PLD method on HOPG substrates depend on deposition and annealing conditions and can vary from a set of grains with different orientations to an epitaxial film. We demonstrate that PLD in vacuum results in damage of the substrate and therefore cannot be used for vdW epitaxy. Instead, PLD at a moderate inert gas pressure followed by annealing at temperatures $T_a \approx 200$ –250 °C enables vdW epitaxy of ultrathin crystalline films of Bi₂Te₃. The nature of a CDW-like surface reconstruction observed on the initial stage of film sublimation needs further study.

Acknowledgments. The SEM measurements were performed using equipment of the Shared Facility Center at P. N. Lebedev Physical Institute of RAS. The computations in this study were performed using computational resources at the Joint Supercomputer Center, Russian Academy of Science. The financial support from the state task and RFBR (grant #19-02-00593) is acknowledged.

References

- [1] CB Satterthwaite and RW Ure Jr. Electrical and thermal properties of Bi₂Te₃. *Physical review*, 108(5):1164, 1957. doi: 10.1103/PhysRev.108.1164. URL <https://link.aps.org/doi/10.1103/PhysRev.108.1164>.
- [2] YL Chen, James G Analytis, J-H Chu, ZK Liu, S-K Mo, Xiao-Liang Qi, HJ Zhang, DH Lu, Xi Dai, Zhong Fang, et al. Experimental realization of a three-dimensional topological insulator. Bi₂Te₃. *Science*, 325(5937):178–181, 2009. doi: 10.1126/science.1173034. URL <https://www.science.org/doi/abs/10.1126/science.1173034>.
- [3] Binghai Yan and Shou-Cheng Zhang. Topological materials. *Reports on Progress in Physics*, 75(9):096501, aug 2012. doi: 10.1088/0034-4885/75/9/096501. URL <https://doi.org/10.1088/0034-4885/75/9/096501>.
- [4] Y.S. Hor, J.G. Checkelsky, D. Qu, N.P. Ong, and R.J. Cava. Superconductivity and non-metallicity induced by doping the topological insulators Bi₂Se₃ and Bi₂Te₃. *Journal of Physics and Chemistry of Solids*, 72(5):572–576, 2011. doi: <https://doi.org/10.1016/j.jpcs.2010.10.027>. URL <https://www.sciencedirect.com/science/article/pii/S0022369710003318>.
- [5] Cui-Zu Chang, Jinsong Zhang, Xiao Feng, Jie Shen, Zuocheng Zhang, Minghua Guo, Kang Li, Yunbo Ou, Pang Wei, Li-Li Wang, Zhong-Qing Ji, Yang Feng, Shuaihua Ji, Xi Chen, Jinfeng Jia, Xi Dai, Zhong Fang, Shou-Cheng Zhang, Ke He, Yayu Wang, Li Lu, Xu-Cun Ma, and Qi-Kun Xue. Experimental observation of the quantum anomalous hall effect in a magnetic topological insulator. *Science*, 340(6129):167–170, 2013. ISSN 0036-8075. doi: 10.1126/science.1234414. URL <https://science.sciencemag.org/content/340/6129/167>.
- [6] Dimitrie Culcer, Aydın Cem Keser, Yongqing Li, and Grigory Tkachov. Transport in two-dimensional topological materials: recent developments in experiment and theory. *2D Materials*, 7(2):022007, mar 2020. doi: 10.1088/2053-1583/ab6ff7. URL <https://doi.org/10.1088/2053-1583/ab6ff7>.
- [7] K. S. Novoselov, D. Jiang, F. Schedin, T. J. Booth, V. V. Khotkevich, S. V. Morozov, and A. K. Geim. Two-dimensional atomic crystals. *Proceedings of the National Academy of Sciences*, 102(30):10451–10453, 2005. ISSN 0027-8424. doi: 10.1073/pnas.0502848102. URL <https://www.pnas.org/content/102/30/10451>.

- [8] Atsushi Koma, Kazumasa Sunouchi, and Takao Miyajima. Fabrication and characterization of heterostructures with subnanometer thickness. *Microelectronic Engineering*, 2(1):129–136, 1984. ISSN 0167-9317. doi: [https://doi.org/10.1016/0167-9317\(84\)90057-1](https://doi.org/10.1016/0167-9317(84)90057-1). URL <https://www.sciencedirect.com/science/article/pii/S0167931784900571>. Special Issue on Nanometer Structure Electronics.
- [9] Jeehwan Kim, Can Bayram, Hongsik Park, Cheng-Wei Cheng, Christos Dimitrakopoulos, John A. Ott, Kathleen B. Reuter, Stephen W. Bedell, and Devendra K. Sadana. Principle of direct van der Waals epitaxy of single-crystalline films on epitaxial graphene. *Nature Communications*, 5(1):4836, 2014. doi: <https://doi.org/10.1038/ncomms5836>.
- [10] J. Krumrain, G. Mussler, S. Borisova, T. Stoica, L. Plucinski, C.M. Schneider, and D. Grützmacher. MBE growth optimization of topological insulator Bi₂Te₃ films. *Journal of Crystal Growth*, 324(1):115–118, 2011. doi: <https://doi.org/10.1016/j.jcrysgro.2011.03.008>. URL <https://www.sciencedirect.com/science/article/pii/S0022024811002806>.
- [11] Guang Wang, Xie-Gang Zhu, Yi-Yang Sun, Yao-Yi Li, Tong Zhang, Jing Wen, Xi Chen, Ke He, Li-Li Wang, Xu-Cun Ma, et al. Topological insulator thin films of Bi₂Te₃ with controlled electronic structure. *Advanced Materials*, 23(26):2929–2932, 2011. doi: <https://doi.org/10.1002/adma.201100678>. URL <https://onlinelibrary.wiley.com/doi/abs/10.1002/adma.201100678>.
- [12] Anupam Roy, Samaresh Guchhait, Sushant Sonde, Rik Dey, Tanmoy Pramanik, Amrithes Rai, Hema CP Movva, Luigi Colombo, and Sanjay K Banerjee. Two-dimensional weak anti-localization in Bi₂Te₃ thin film grown on Si (111)-(7×7) surface by molecular beam epitaxy. *Applied Physics Letters*, 102(16):163118, 2013. doi: <https://doi.org/10.1063/1.4803018>. URL <https://doi.org/10.1063/1.4803018>.
- [13] X Liu, DJ Smith, J Fan, Y-H Zhang, H Cao, YP Chen, J Leiner, Brian J Kirby, M Dobrowolska, and JK Furdyna. Structural properties of Bi₂Te₃ and Bi₂Se₃ topological insulators grown by molecular beam epitaxy on GaAs(001) substrates. *Applied Physics Letters*, 99(17):171903, 2011. doi: <https://doi.org/10.1063/1.3655995>. URL <https://doi.org/10.1063/1.3655995>.
- [14] SE Harrison, S Li, Y Huo, B Zhou, YL Chen, and JS Harris. Two-step growth of high quality Bi₂Te₃ thin films on Al₂O₃ (0001) by molecular beam epitaxy. *Applied Physics Letters*, 102(17):171906, 2013. doi: <https://doi.org/10.1063/1.4803717>. URL <https://doi.org/10.1063/1.4803717>.
- [15] Rita J Macedo, Sara E Harrison, Tatiana S Dorofeeva, James S Harris, and Richard A Kiehl. Nanoscale probing of local electrical characteristics on mbe-grown Bi₂Te₃ surfaces under ambient conditions. *Nano letters*, 15(7):4241–4247, 2015. doi: <https://doi.org/10.1021/acs.nanolett.5b00542>. URL <https://doi.org/10.1021/acs.nanolett.5b00542>. PMID: 26030139.
- [16] Gilberto Rodrigues-Junior, Lucas Atila Bernardes Marçal, Guilherme AS Ribeiro, Paulo Henrique de Oliveira Rappl, Eduardo Abramof, Paulo Vitor Sciammarella, Luciano de Moura Guimarães, Carlos Alberto Pérez, and Ângelo Malachias. Direct observation of large strain through van der Waals gaps on epitaxial Bi₂Te₃/graphite: Pseudomorphic relaxation and the role of Bi₂ layers on the Bi_xTe_y topological insulator series. *Physical Review Materials*, 4(2):023602, 2020. doi: <https://doi.org/10.1103/PhysRevMaterials.4.023602>. URL <https://link.aps.org/doi/10.1103/PhysRevMaterials.4.023602>.
- [17] Douglas B. Chrisey and Graham K. Hubler. *Pulsed Laser Deposition of Thin Films*. 2003.
- [18] A Dauscher, A Thomy, and H Scherrer. Pulsed laser deposition of Bi₂Te₃ thin films. *Thin solid films*, 280(1-2):61–66, 1996. doi: [https://doi.org/10.1016/0040-6090\(95\)08221-2](https://doi.org/10.1016/0040-6090(95)08221-2). URL <https://www.sciencedirect.com/science/article/pii/S0040609095082212>.
- [19] Alessandro Bailini, Fabio Donati, M Zamboni, Valeria Russo, Matteo Passoni, Carlo Spartaco Casari, A Li Bassi, and Carlo Enrico Bottani. Pulsed laser deposition of Bi₂Te₃ thermoelectric films. *Applied Surface Science*, 254(4):1249–1254, 2007. doi: <https://doi.org/10.1016/j.apsusc.2007.09.039>. URL <https://www.sciencedirect.com/science/article/pii/S0169433207013414>.
- [20] Haruhiko Obara, Shun Higomo, Michihiro Ohta, Atsushi Yamamoto, Kazuo Ueno, and Tsutomu Iida. Thermoelectric properties of Bi₂Te₃-based thin films with fine grains fabricated by pulsed laser deposition. *Japanese Journal of Applied Physics*, 48(8R):085506, 2009. doi: <https://doi.org/10.1143/jjap.48.085506>. URL <https://doi.org/10.1143/jjap.48.085506>.
- [21] YS Wudil, MA Gondal, SG Rao, S Kunwar, and AQ Alsayoud. Substrate temperature-dependent thermoelectric figure of merit of nanocrystalline Bi₂Te₃ and Bi₂Te_{2.7}Se_{0.3} prepared using pulsed laser deposition supported by dft study. *Ceramics International*, 46(15):24162–24172, 2020. doi: <https://doi.org/10.1016/j.ceramint.2020.06.196>. URL <https://www.sciencedirect.com/science/article/pii/S0272884220318563>.
- [22] SX Zhang, L Yan, J Qi, M Zhuo, Y-Q Wang, RP Prasankumar, QX Jia, and ST Picraux. Epitaxial thin films of topological insulator Bi₂Te₃ with two-dimensional weak anti-localization effect grown by pulsed laser deposition. *Thin Solid Films*, 520(21):6459–6462, 2012. doi: <https://doi.org/10.1016/j.tsf.2012.07.012>. URL <https://www.sciencedirect.com/science/article/pii/S0040609012008619>.
- [23] Zhenwei Yu, Xiaolin Wang, Yi Du, Sima Aminoroaya-Yamni, Chao Zhang, Kris Chuang, and Sean Li. Fabrication and characterization of textured Bi₂Te₃ thermoelectric thin films prepared on glass substrates at room temperature using pulsed laser deposition. *Journal of crystal growth*, 362:247–251, 2013. doi: <https://doi.org/10.1016/j.jcrysgro.2012.05.045>. URL <https://www.sciencedirect.com/science/article/pii/S0022024812005970>.
- [24] Phuoc Huu Le, Chien-Neng Liao, Chih Wei Luo, and Jihperng Leu. Thermoelectric properties of nanostructured bismuth–telluride thin films grown using pulsed laser deposition. *Journal of alloys and compounds*, 615:546–552, 2014. doi: <https://doi.org/10.1016/j.jallcom.2014.07.018>. URL <https://www.sciencedirect.com/science/article/pii/S0925838814015977>.
- [25] Zhaoliang Liao, Matthew Brahlek, Jong Mok Ok, Lauren Nuckols, Yogesh Sharma, Qiyang Lu, Yanwen Zhang, and Ho Nyung Lee. Pulsed-laser epitaxy of topological insulator Bi₂Te₃ thin films. *APL Materials*, 7(4):041101, 2019. doi: <https://doi.org/10.1063/1.5088190>. URL <https://doi.org/10.1063/1.5088190>.
- [26] Sheng-Rui Jian, Phuoc Huu Le, Chih-Wei Luo, and Jenh-Yih Juang. Nanomechanical and wettability properties of Bi₂Te₃ thin films: Effects of post-annealing. *Journal of Applied Physics*, 121(17):175302, 2017. doi: <https://doi.org/10.1063/1.4982911>. URL <https://doi.org/10.1063/1.4982911>.
- [27] Cheng-Hsun Tasi, Yu-Chin Tseng, Sheng-Rui Jian, Ying-Yen Liao, Chih-Ming Lin, Ping-Feng Yang, Dao-Long Chen, Hsueh-Ju Chen, Chih-Wei Luo, and Jenh-Yih Juang. Nanomechanical properties of Bi₂Te₃ thin films by nanoindentation. *Journal of Alloys and Compounds*, 619:834–838, 2015. doi: <https://doi.org/10.1016/j.jallcom.2014.09.028>. URL <https://www.sciencedirect.com/science/article/pii/S0925838814021628>.
- [28] D. R. Hamann J. Tersoff. Theory of the scanning tunneling microscope. *Phys. Rev. B*, 31:805–813, Jan 1985. doi: <https://doi.org/10.1103/PhysRevB.31.805>. URL <https://journals.aps.org/prb/abstract/10.1103/PhysRevB.31.805>.
- [29] Xi Chen, Xu-Cun Ma, Ke He, Jin-Feng Jia, and Qi-Kun Xue. Molecular beam epitaxial growth of topological insulators. *Advanced Materials*, 23(9):1162–1165, 2011. doi: <https://doi.org/10.1002/adma.201003855>. URL <https://onlinelibrary.wiley.com/doi/abs/10.1002/adma.201003855>.
- [30] Cun Mao, Mingyue Tan, Ligang Zhang, Di Wu, Weiming Bai, and Libin Liu. Experimental reinvestigation and thermodynamic description of Bi-Te binary system. *Calphad*, 60:81–89, 2018. ISSN 0364-5916. doi: <https://doi.org/10.1016/j.calphad.2017.11.007>. URL <https://www.sciencedirect.com/science/article/pii/S0364591617301219>.
- [31] Jinglei Chen, Yawei Dai, Yaqiang Ma, Xianqi Dai, Wingkin Ho, and Maohai Xie. Ultrathin β-tellurium layers grown on highly oriented pyrolytic graphite by molecular-beam epitaxy. *Nanoscale*, 9(41):15945–15948, 2017. URL <https://www.rsc.org/suppdata/c7/nr/c7nr04085g/c7nr04085g1.pdf>.

- [32] KAZUO Yamana, KUNIAKI Kihara, and TAKEO Matsumoto. Bismuth tellurides: BiTe and Bi₄Te₃. *Acta Crystallographica Section B: Structural Crystallography and Crystal Chemistry*, 35(1):147–149, 1979. doi: 10.1107/S0567740879002788. URL <https://doi.org/10.1107/S0567740879002788>.
- [33] Markus Eschbach, Martin Lanius, Chengwang Niu, Ewa Młyńczak, Pika Gospodarič, Jens Kellner, Peter Schüffelgen, Mathias Gehlmann, Sven Döring, Elmar Neumann, Martina Luysberg, Gregor Mussler, Lukasz Plucinski, Markus Morgenstern, Detlev Grützmacher, Gustav Bihlmayer, Stefan Blügel, and Claus M. Schneider. Bi₁te₁ is a dual topological insulator. *Nature Communications*, 8(1):14976, 2017. doi: 10.1038/ncomms14976. URL <https://doi.org/10.1038/ncomms14976>.
- [34] Anubhav Jain, Shyue Ping Ong, Geoffroy Hautier, Wei Chen, William Davidson Richards, Stephen Dacek, Shreyas Cholia, Dan Gunter, David Skinner, Gerbrand Ceder, and Kristin a. Persson. The Materials Project: A materials genome approach to accelerating materials innovation. *APL Materials*, 1(1):011002, 2013. ISSN 2166532X. doi: 10.1063/1.4812323. URL <http://link.aip.org/link/AMPADS/v1/i1/p011002/s1&Agg=doi>.
- [35] Xie-Gang Zhu, Yun Zhang, Wei Feng, Bing-Kai Yuan, Qin Liu, Rui-Zhi Qiu, Dong-Hua Xie, Shi-Yong Tan, Yu Duan, Yun Fang, Wen Zhang, and Xin-Chun Lai. Electronic structures of topological insulator Bi₂Te₃ surfaces with non-conventional terminations. *New Journal of Physics*, 18(9):093015, sep 2016. doi: 10.1088/1367-2630/18/9/093015. URL <https://doi.org/10.1088/1367-2630/18/9/093015>.
- [36] F. Izumi K. Momma. Vesta 3 for three-dimensional visualization of crystal, volumetric and morphology data. *J App. Cryst.*, 44:1272–1276, Dec 2011. doi: 10.1107/S0021889811038970. URL <https://onlinelibrary.wiley.com/doi/full/10.1107/S0021889811038970?sentby=iucr>.
- [37] Y. Franghiadakis, C. Fotakis, and P. Tzanetakis. Energy distribution of ions produced by excimer-laser ablation of solid and molten targets. *Applied Physics A*, 68(4):391–397, 1999. doi: 10.1007/s003390050911. URL <https://doi.org/10.1007/s003390050911>.